

# Designing magnetocaloric materials for hydrogen liquefaction with light rare-earth Laves phases

Wei Liu<sup>1,\*</sup>, Tino Gottschall<sup>2</sup>, Franziska Scheibel<sup>1</sup>, Eduard Bykov<sup>2,3</sup>, Nuno Fortunato<sup>1</sup>, Alex Aubert<sup>1</sup>, Hongbin Zhang<sup>1</sup>, Konstantin Skokov<sup>1</sup>, and Oliver Gutfleisch<sup>1</sup>

<sup>1</sup>Institute of Materials Science, Technical University of Darmstadt, 64287 Darmstadt, Germany

<sup>2</sup>Dresden High Magnetic Field Laboratory (HLD-EMFL) and Würzburg-Dresden Cluster of Excellence ct.qmat, Helmholtz-Zentrum Dresden-Rossendorf, 01328 Dresden, Germany

<sup>3</sup>Institute of Solid State and Materials Physics, Technische Universität Dresden, 01062 Dresden, Germany

\*Author to whom correspondence should be addressed: [wei.liu@tu-darmstadt.de](mailto:wei.liu@tu-darmstadt.de) Alarich-Weiss-str. 16, 64287 Darmstadt

## Abstract

Magnetocaloric hydrogen liquefaction could be a “game-changer” for liquid hydrogen industry. Although heavy rare-earth based magnetocaloric materials show strong magnetocaloric effects in the temperature range required by hydrogen liquefaction (77 ~ 20 K), the high resource criticality of the heavy rare-earth elements is a major obstacle for upscaling this emerging liquefaction technology. In contrast, the higher abundances of the light rare-earth elements make their alloys highly appealing for magnetocaloric hydrogen liquefaction. Via a mean-field approach, it is demonstrated that tuning the Curie temperature ( $T_C$ ) of an idealized light rare-earth based magnetocaloric material towards lower cryogenic temperatures leads to larger maximum magnetic and adiabatic temperature changes ( $\Delta S_T$  and  $\Delta T_{ad}$ ). Especially in the vicinity of the condensation point of hydrogen (20 K),  $\Delta S_T$  and  $\Delta T_{ad}$  of the optimized light rare-earth based material are predicted to show significantly large values. Following the mean-field approach and taking the chemical and physical similarities of the light rare-earth elements into consideration, a method of designing light rare-earth intermetallic compounds for hydrogen liquefaction is used: tuning  $T_C$  of a rare-earth alloy to approach 20 K by mixing light rare-earth elements with different *de Gennes* factors. By mixing Nd and Pr in Laves phase (Nd,Pr)Al<sub>2</sub>, and Pr and Ce in Laves phase (Pr, Ce)Al<sub>2</sub>, a fully light rare-earth intermetallic series with large magnetocaloric effects covering the temperature range required by hydrogen liquefaction is developed, demonstrating a competitive maximum effect compared to the heavy rare-earth compound DyAl<sub>2</sub>.

Keywords: Magnetism, Magnetic Materials, Magnetocaloric, Magnetic Refrigeration, Hydrogen Energy, Hydrogen Liquefaction

## 1. Introduction

Discovered in 1917 by Weiss and Picard, magnetocaloric effect is a cooling or warming effect of a magnetic material being exposed to a magnetic field [1]. Soon after its discovery, magnetic cooling has been successfully applied to attaining extremely low temperature [2, 3]. In 1949, the Nobel prize in chemistry was awarded to Giauque, who developed a magnetic refrigeration device to approach absolute zero [4].

Nowadays, global climate change caused by greenhouse-gas emissions threatens human civilization with grave consequences. In order to achieve climate-neutrality, new

energy concepts emphasizing technologies that improve energy efficiency, or replace fossil fuels are required [5]. Ideally releasing no pollutants and greenhouse gases, green hydrogen is finally set to be the fuel for the future [6–8]. Hydrogen liquefaction is important for efficient storage and transportation of hydrogen energy [7, 9, 10]. However, liquid hydrogen is expensive due to the low efficiency of the conventional liquefaction technologies based on Joule-Thomson expansion [11, 12]. Recently, there is a growing interest in magnetocaloric liquefaction for hydrogen and other industrial gases [13–25]. The emerging magnetocaloric liquefaction technology is in principle more efficient [5, 26–

32], making the promise of hydrogen fuel being affordable for the society to reach climate-neutrality.

If pre-cooled by liquid nitrogen, the temperature range required by magnetocaloric hydrogen liquefaction is from 77 (condensation point of nitrogen) to 20 K (condensation point of hydrogen). For the success of a practical application of magnetocaloric hydrogen liquefaction on an industrial scale, affordable magnetocaloric materials with large isothermal magnetic entropy and adiabatic temperature changes ( $\Delta S_T$  and  $\Delta T_{ad}$ ) in the target temperature regime under affordable magnetic fields are needed [33–38]. In this work, we focus on the criticality of raw elements, the two physical quantities  $\Delta S_T$  and  $\Delta T_{ad}$  in temperature range of 77 ~ 20 K under magnetic field changes such as 2 T, which can be realized by Nd-Fe-B permanent magnets [5], or 5 T, which can be generated by commercial superconducting magnets [32].

Rare-earth based magnetocaloric materials are one big family of the magnetocaloric materials for hydrogen liquefaction [37, 39, 40]. Lanthanide rare-earth elements can be divided into two major groups: light rare-earth elements (La, Ce, Pr, Nd, Sm) and heavy rare-earth elements (Gd, Tb, Dy, Ho, Er, Tm, Yb, Lu). Putting aside the criticality of the raw materials for a moment, heavy rare-earth based magnetocaloric materials would be strong contenders for magnetocaloric hydrogen liquefaction in the context of performance. Materials such as HoB<sub>2</sub> [15, 41, 42], ErCo<sub>2</sub> [43,

44], DyAl<sub>2</sub> [45], and ErAl<sub>2</sub> [45, 46] show large  $\Delta S_T$  and  $\Delta T_{ad}$  due to the large magnetic moments of the heavy rare-earth ions, and they are often proposed to be used in an active magnetic regenerator for hydrogen liquefaction. Because of the excellent magnetocaloric properties, heavy rare-earth based materials are intensively studied.

In contrast, light rare-earth based magnetocaloric materials for hydrogen liquefaction are less investigated since their magnetocaloric effects are usually weaker due to their smaller magnetic moments [45]. **Figure 1** (a) shows the theoretical effective magnetic moment  $\mu_{eff}$  and the *de Gennes* factor ( $G$ ) of the rare-earth ions [47]. The rare-earth ions are divided into three categories, namely the light rare-earth ions, Eu<sup>3+</sup>, and the heavy rare-earth ions. Pr<sup>3+</sup> has the highest theoretical  $\mu_{eff}$  of 3.58  $\mu_B$  among the light rare-earth ions, whereas the heavy rare-earth ions from Gd<sup>3+</sup> to Tm<sup>3+</sup> have a theoretical  $\mu_{eff}$  larger than 7.5  $\mu_B$ .

However, the criticality of the raw materials cannot be ignored for a viable industrial-scale application. The consumption of H<sub>2</sub> in EU is predicted to reach 2250 TWh/year by 2050 according to Hydrogen Roadmap Europe [48]. If about one-third of H<sub>2</sub> needs to be transported and stored in its liquid state, one would require about 13,000 small-scale liquefaction plants with a production capacity of 5 tons per day. Providing a potential hydrogen liquefier using

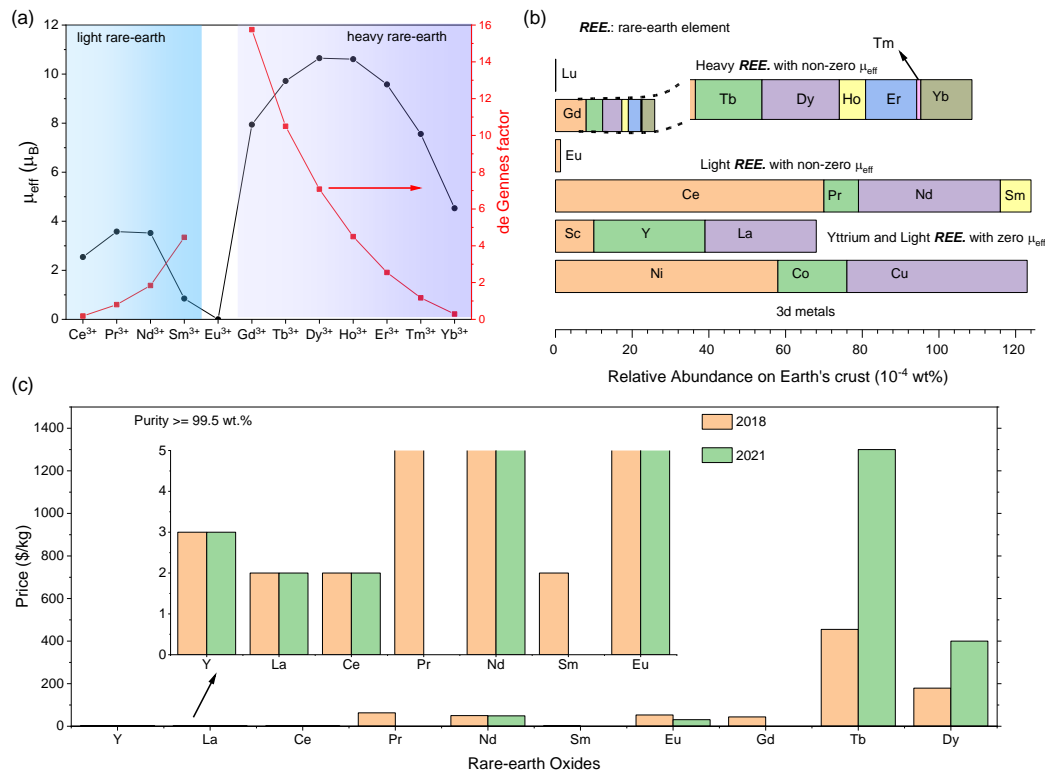


**Figure 1** (a) Effective magnetic moments and *de Gennes* factors of the rare-earth ions [47]. (b) relative abundance of Ni, Co, Cu, and the rare-earth elements which are categorized into non-heavy rare-earth elements with zero magnetic moments (Sc, Y, La), light rare-earth elements with non-zero magnetic moments (Ce, Pr, Nd, Sm), Eu, and heavy rare-earth elements with non-zero magnetic moments (Gd, Tb, Dy, Ho, Er, Tm, Yb), and zero magnetic moments (Lu). Data are taken from Ref.[53]. (c) Prices of the rare-earth oxides (Y, La, Ce, Pr, Nd, Sm, Eu, Gd, Tb, Dy) in year 2018 and 2021. Data are taken from Ref. [54, 55].

magnetocaloric material  $\text{HoAl}_2$  as the refrigerant for the final cooling state operating at 20 K at a frequency of 1 Hz in fields of 7 T, about 1 ton of holmium would be needed [49]. This means a total of 13,000 tons for the EU alone, and the total holmium production is a measly 10 tons per year [50].

Heavy rare-earth elements belong to the highly critical elements [51, 52]. One contribution to the high criticalities is their poor abundances on the earth's crust. **Figure 1** (b) shows the relative abundances of Ni, Co, Cu, and the rare-earth elements on the earth's crust [53]. Heavy rare-earth elements such as Tb, Ho, Tm, and Lu are not abundant, whereas light rare-earth metal Ce is even more abundant than Cu, and light rare-earth elements La and Nd, and Y are more abundant than Co. The total abundances of the heavy rare-earth elements combined are not as rich as that of Nd alone. **Figure 1** (c) plots the prices (always volatile) of the rare-earth oxides in year 2018 and 2021 for Y, La, Ce, Pr, Nd, Sm, Eu, Gd, Tb, and Dy [54, 55]. The prices of the heavy rare-earth oxides, namely for Tb, Dy, are over 400 \$/kg in 2021, whereas the prices of the Pr and Nd oxides are around 50 \$/kg, and the prices of Y, La, Ce, Sm oxides are just several dollars per kg. Eu and Gd oxides are also relatively cheap in comparison with Tb and Dy oxides. This is because they are not as largely used in industry as Tb and Dy.

It needs to be emphasized that criticality is much more than just simple geological abundances. Factors such as mining, beneficiation, hazardous by-products, separation (and their social and ecological consequences along this value chain), geopolitics, trade restrictions and monopolistic supply in terms of demand vs. supply, need to be understood and quantified in terms of LCA (Life-Cycle-Analysis) and LCC (Life-Cycle-Costing) [56]. Nevertheless, the discussion above points out that the high criticality of the heavy rare-earth elements questions the feasibility of using heavy rare-earth based magnetocaloric materials for hydrogen liquefaction in a viable industrial scale [57, 58]. Taking the dominant abundance of the light rare-earth elements over the heavy rare-earth elements into consideration, it is more feasible to use light rare-earth based magnetocaloric materials for hydrogen liquefaction. In this work, we aim at developing a light rare-earth based material system with sufficient magnetocaloric effects covering a full temperature range (77 ~ 20 K) required by magnetocaloric hydrogen liquefaction.

It is worth mentioning that much work has been done on tuning the transition temperature of heavy rare-earth magnetocaloric materials. Mixing two different heavy rare-earth elements on the rare-earth sites is a widely used method. Examples are several works on heavy rare-earth Laves phases  $\text{RNi}_2$ ,  $\text{RAl}_2$ , and  $\text{RCO}_2$  (R: rare-earth element) systems: the  $\text{Dy}_{1-x}\text{Er}_x\text{Ni}_2$  ( $x = 0.25, 0.5, 0.75$ ) [59], the  $\text{Tb}_{1-x}\text{Er}_x\text{Ni}_2$  ( $x = 0.75, 0.5, 0.25$ ) [60], the  $\text{Tb}_{1-x}\text{Ho}_x\text{Ni}_2$  ( $x = 0.25, 0.5, 0.75$ ) [61], the  $\text{Ho}_{1-x}\text{Er}_x\text{Ni}_2$  ( $x = 0.25, 0.5, 0.75$ ) [62], the  $\text{Tm}_x\text{Dy}_{1-x}\text{Al}_2$  ( $0 \leq x \leq 1$ ) [13], the  $(\text{Er}_x\text{R}_{1-x})\text{Co}_2$  (R=Ho, Dy;  $0 \leq x \leq 1$ ) [63] and

the  $\text{Er}_x\text{Dy}_{1-x}\text{Al}_2$  ( $x = 0.45, 0.67, 0.9$ ) [64]. Following these studies, we apply this method to the light rare-earth Laves phases: mixing different light rare-earth elements on the rare-earth sites to tune the transition temperature within 20 ~ 77 K for magnetocaloric hydrogen liquefaction.

## 2. Mean-field Approach

Inspired by the sharply increasing trends of  $\Delta S_T$  and  $\Delta T_{ad}$  with decreasing  $T_C$  in the vicinity of the condensation point of hydrogen (20 K) for heavy rare-earth based magnetocaloric materials demonstrated by a mean-field approach from our previous work (Ref. [45]), we focus in this work on the light rare-earth based magnetocaloric materials. We continue to develop the mean-field approach used in the aforementioned work, where the detailed description can be found [45]. It is worth mentioning that using the mean-field model to describe the magnetocaloric properties is a well-known method, as used in Ref. [65–69]. In some studies, also effects related to the crystalline electric field are taken into consideration [70–72]. In this work, we aimed at providing a simple way to understand the sharply increasing feature of magnetocaloric effect of the light rare-earth magnetocaloric materials with a Curie temperature in the vicinity of hydrogen condensation point.

The total entropy change  $S$  of a magnetocaloric material is contributed by three items, namely the magnetic entropy  $S_m$ , the lattice entropy  $S_l$ , and the electronic entropy  $S_e$ :

$$S = S_m + S_l + S_e, \quad (1)$$

The equation to calculate the magnetic entropy is given as [73]:

$$S_m = N_M k_B \left[ \ln \left( \frac{\sinh \frac{2J+1}{2J} x}{\sinh \frac{1}{2J} x} \right) - x B_J(x) \right], \quad (2)$$

with  $x = \frac{\mu \mu_0 H + \frac{3J}{J+1} k_B T_C B_J(x)}{k_B T}$ .  $H$  is the magnetic field,  $J$  the total angular momentum,  $N_M$  the number of “magnetic atoms”,  $k_B$  the Boltzmann constant,  $\mu$  the atomic magnetic moment,  $T_C$  the Curie temperature,  $\mu_0$  the vacuum permeability, and  $B_J(x)$  the Brillouin function. A more detailed description on Equation (2) can be found in Ref. [73]. The lattice entropy is given as [73]:

$$S_l = -3Nk_B \left[ 1 - \exp \left( -\frac{T_D}{T} \right) \right] + 12Nk_B \left( \frac{T}{T_D} \right)^3 \int_0^{\frac{T_D}{T}} \frac{x^3}{\exp(x) - 1} dx. \quad (3)$$

where  $T_D$  is the Debye temperature,  $N$  the total number of atoms, and  $x$  can be regarded as a variable in the range of  $0 \sim T_D/T$ . The electronic entropy is given by [73]

$$S_e = \int_0^T \frac{C_e}{T} dT = \gamma T, \quad (4)$$

where  $\gamma$  is the Sommerfeld coefficient and  $C_e$  is the electronic heat capacity ( $C_e = \gamma T$ ). In the present work,  $S_e$  is neglected out of simplification, since mostly  $C_e$  is dominant only at sufficiently low temperatures [74].

Constructing the total entropy  $S(T, H)$  curves by summing  $S_m$  and  $S_l$ , the isothermal magnetic and adiabatic temperature changes ( $\Delta S_T$  and  $\Delta T_{ad}$ ) are given by [73]

$$\begin{aligned} \Delta S_T(T, H) &= S(T, H) - S(T, 0), \\ \Delta T_{ad}(T, H) &= T(S, H) - T(S, 0), \end{aligned} \quad (5)$$

where  $T(S, H)$  is the inverse function of  $S(T, H)$ . More details on Equation (1)~(5) can be found in Ref. [73].

We assume an idealized Nd- alloy family with the  $T_C$  of its alloys varying from 300 K to 10 K and the other parameters, namely  $J$ ,  $\mu_{eff}$ , and  $T_D$ , staying constant. For comparisons, we assume an idealized Dy- alloy family correspondingly. For the light rare-earth alloy series,  $J$  and  $\mu_{eff}$  are taken to be 4.5 and  $3.52 \mu_B$  respectively, corresponding to the  $\text{Nd}^{3+}$  ion. For the heavy rare-earth alloy series,  $J$  and  $\mu_{eff}$  are taken to be 7.5 and  $10 \mu_B$  respectively, corresponding to the  $\text{Dy}^{3+}$  ion.  $T_D$  of the light rare-earth alloy series is assumed to be 352 K, which corresponds to Laves phase  $\text{LaAl}_2$  [75]. For the heavy rare-earth alloy series,  $T_D$  is assumed to be 384 K, which corresponds to Laves phase  $\text{LuAl}_2$  [75].  $\Delta S_T(T, H)$  and  $\Delta T_{ad}(T, H)$  can be calculated by Equation (5).

**Figure 2** (a) shows the  $\Delta S_T(T)$  of the Nd- alloy family, and the maximum  $\Delta S_T$  of the Dy- alloy family in magnetic fields of 5 T. In the temperature range of 77 ~ 20 K, the maximum  $\Delta S_T$  of the light rare-earth alloy series are large. Especially in the vicinity of the condensation point of hydrogen (20 K), ‘‘giant’’ values are observed, being almost two times larger than those of the heavy rare-earth alloys with a  $T_C$  near room temperature. **Figure 2** (b) shows the  $\Delta T_{ad}(T)$  of the Nd- alloy family, and the maximum  $\Delta T_{ad}$  of the Dy- alloy family in magnetic fields of 5 T. Near 20 K, the light rare-earth alloy series shows a considerable maximum  $\Delta T_{ad}$ , which is larger than or comparable to that of the heavy rare-earth alloys with a  $T_C$  near room temperature. Both  $\Delta S_T$  and  $\Delta T_{ad}$  show an increasing maximum value with a decreasing  $T_C$  in the temperature range of 77 ~ 20 K. As predicted by the calculations, we can see that the light rare-earth series also achieve a large  $\Delta S_T$  and  $\Delta T_{ad}$  at low cryogenic temperatures, especially in the vicinity of the condensation point of hydrogen.

The calculations above point out a way of designing a fully light rare-earth based magnetocaloric materials for hydrogen liquefaction: tune the  $T_C$  down to 20 K. Though there are no such idealized alloy families where only  $T_C$

varies, the chemical and physical similarities of the light rare-earth elements, namely Ce, Pr, and Nd, makes it easy to tune the  $T_C$  of their alloys by mixing different rare-earth elements with different *de Gennes* factors on the rare-earth sublattices [76–78], as  $T_C$  of rare-earth based alloys usually scales with *de Gennes* factor following the equation

$$T_C = \frac{2ZJG}{3k_B}, \quad (6)$$

where  $Z$  is the nearest neighbors,  $J$  is the Heisenberg exchange constant, and  $G$  is the *de Gennes* factor [47].

It has been reported that Laves phases  $\text{NdAl}_2$  with a  $T_C$  near 77 K and  $\text{PrAl}_2$  with a  $T_C$  near 30 K are two magnetocaloric materials with a large  $\Delta S_T$  and  $\Delta T_{ad}$  [70]. However, these two compounds are unable to cover the full temperature range of 77 ~ 20 K. As shown in **Figure 1** (a), the *de Gennes* factor of Nd, Pr, and Ce are significantly different, decreasing from 1.84 for Nd to 0.18 for Ce. Based on the analyses above, we predict that a light rare-earth  $\text{RAl}_2$  (R: rare-earth elements) Laves phase series that covers the full temperature range (77 ~ 20 K) required by magnetocaloric

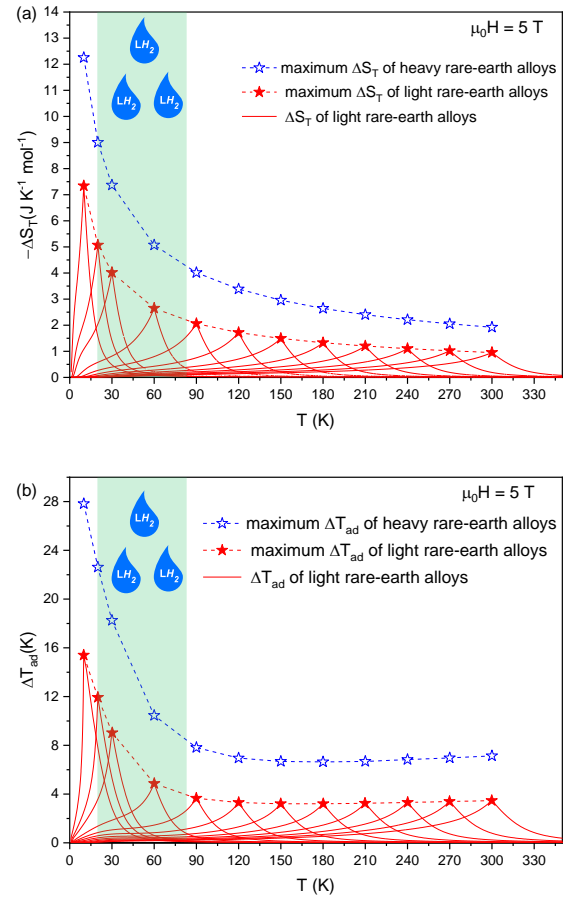


**Figure 2** (a) Magnetic entropy and (b) adiabatic temperature changes of a light rare-earth alloy series (idealized Nd- alloy family) and the maximum magnetic entropy and adiabatic temperature changes of the heavy rare-earth alloy series (idealized Dy- alloy family) from mean-field approach. Light green shadows marks the temperature range required by magnetocaloric hydrogen liquefaction.

hydrogen liquefaction can be realized by tuning the  $T_c$  via mixing Pr and Nd in (Nd,Pr)Al<sub>2</sub>, and Pr and Ce in (Pr,Ce)Al<sub>2</sub>.

### 3. Experiment

Polycrystalline Nd<sub>x</sub>Pr<sub>1-x</sub>Al<sub>2</sub> ( $x = 1, 0.75, 0.5, 0.25$ ) and Pr<sub>x</sub>Ce<sub>1-x</sub>Al<sub>2</sub> ( $x = 1, 0.75, 0.5, 0.25$ ) samples were synthesized by arc melting high-purity elements Ce (99.5 at. %), Pr (99.5 at. %), Nd (99.5 at. %), and Al (99.998 at. %) under Ar atmosphere. We did not synthesize Pr<sub>0.25</sub>Ce<sub>0.75</sub>Al<sub>2</sub> and CeAl<sub>2</sub> since the later magnetization measurements show that the transition temperature of Pr<sub>0.5</sub>Ce<sub>0.5</sub>Al<sub>2</sub> is already below 20 K. To ensure good homogeneity, all the samples were melted three times. The ingots were turned upside down before each melting step. Evaporation of the rare-earth elements was negligible. Powder X-ray diffraction (XRD) patterns were collected at room temperature with an x-ray diffractometer (Stadi P, Stoe & Cie GmbH) equipped with a Ge[111]-Monochromator using Mo-K $\alpha$ -radiation in the Debye-Scherrer geometry. The XRD data were evaluated by Rietveld refinement with the FullProf software packages [79]. Backscatter electron (BSE) images were collected with a Tescan Vega 3 scanning electron microscope (SEM). A Physical Properties Measurement System (PPMS) from Quantum Design was used to measure the magnetization of the samples in magnetic fields up to 5 T. Heat capacity in magnetic fields of 0, 2, and 5 T was measured in the same PPMS with the  $2\tau$  approach.

## 4. Results and discussions

### 4.1 Phase characterization

The Laves phases NdAl<sub>2</sub> and PrAl<sub>2</sub> crystallize in the MgCu<sub>2</sub> cubic structure (space group: 227). **Figure 3** (a) shows the XRD patterns of the (R<sub>1</sub>,R<sub>2</sub>)Al<sub>2</sub> (R<sub>1</sub>: Nd, Pr, R<sub>2</sub>: Pr, Ce) samples. Detailed Rietveld refinements are included in the supplementary. The Rietveld refinements confirm that (Nd,Pr)Al<sub>2</sub> and (Pr,Ce)Al<sub>2</sub> does not change their crystal structures with the variation of Nd, Pr, or Ce content. Phase fraction analyses demonstrate the high quality of all the samples since the impurities are undetectable. The lattice constants of (Nd,Pr)Al<sub>2</sub> and (Pr,Ce)Al<sub>2</sub> samples are plotted in **Figure 3** (b). The lattice constants increase almost linearly with increasing Pr content in (Nd,Pr)Al<sub>2</sub> series and increasing Ce content in (Pr, Ce)Al<sub>2</sub> series, respectively. This is coherent with the fact that CeAl<sub>2</sub> has the largest and NdAl<sub>2</sub> has the smallest lattice constant [78]. The quality of all the samples is further confirmed by SEM imaging. **Figure 3** (c) shows an example of the microscopy using BSE contrast, proving phase purity of the Pr<sub>0.75</sub>Ce<sub>0.25</sub>Al<sub>2</sub> sample.

### 4.2 Paramagnetic Curie temperature

**Figure 4** (a) plots the magnetization measurements of the Laves phases (R<sub>1</sub>,R<sub>2</sub>)Al<sub>2</sub> (R<sub>1</sub>: Nd, Pr, R<sub>2</sub>: Pr, Ce) as a function of temperature in magnetic fields of 5 T to check the saturation magnetization. The samples were firstly cooled down to 7 K in magnetic fields of 5 T, and then heated up with their

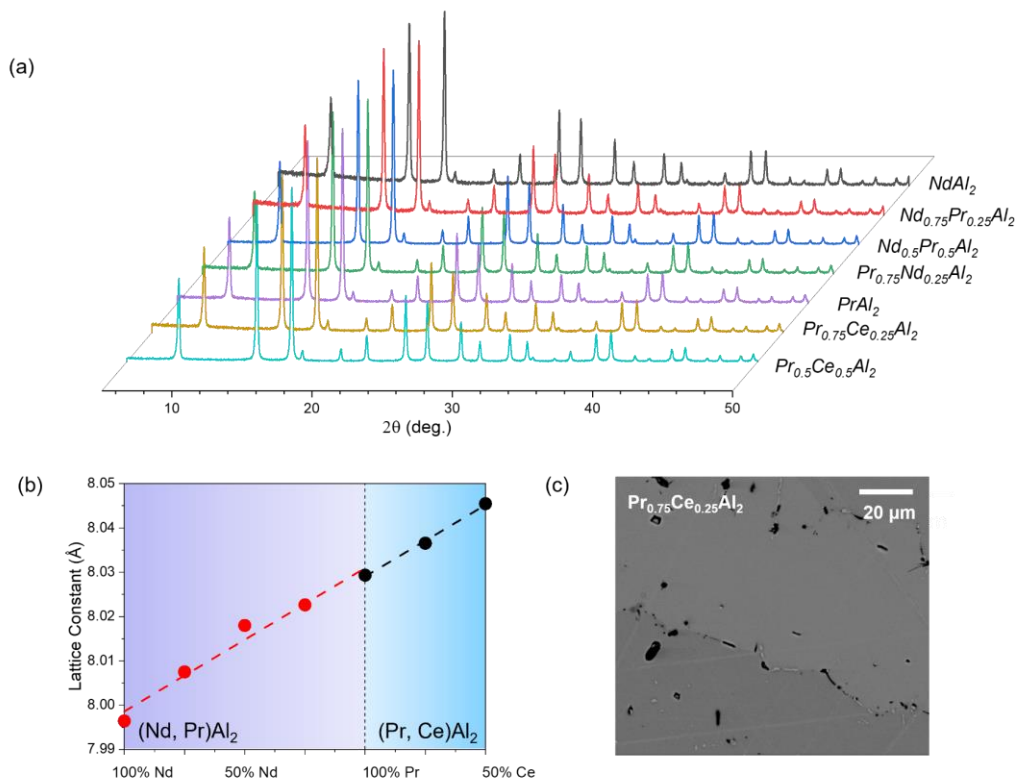


**Figure 3** (a) XRD patterns of the Laves phases (R<sub>1</sub>,R<sub>2</sub>)Al<sub>2</sub> (R<sub>1</sub>: Nd, Pr, R<sub>2</sub>: Pr, Ce) measured at room temperature. (b) Lattice constants of all the samples given by Rietveld refinement. The red dashed line is the linear fitting for (Nd, Pr)Al<sub>2</sub> samples, and the black line dashed line is the linear fitting for (Pr, Ce)Al<sub>2</sub> samples. (c) BSE image of Pr<sub>0.75</sub>Ce<sub>0.25</sub>Al<sub>2</sub>. The black dots are holes.

magnetization measured in parallel. Under the same cooling and heating procedures, magnetization measurements in 0.1 T were done, the results are included in the supplementary. The saturated magnetization at 7 K of (Nd,Pr)Al<sub>2</sub> and Pr<sub>0.75</sub>Ce<sub>0.25</sub>Al<sub>2</sub> samples is rather close, in the range between 64 and 71 Am<sup>2</sup>/kg. Pr<sub>0.5</sub>Ce<sub>0.5</sub>Al<sub>2</sub> is the only exception having a significantly lower magnetization of around 40 Am<sup>2</sup>/kg.

**Figure 4** (b) shows the Curie-Weiss fits of all the samples in magnetic fields of 1 T. To reduce the deviation of the reciprocal magnetic susceptibility from the Curie-Weiss behavior, which may be associated with intrinsic factors such as the van Vleck effect, or extrinsic factors such as impurities [80–82], we performed the Curie-Weiss fit in 1 T. The paramagnetic Curie temperature can be determined by the intercepts of the Curie-Weiss fit with the x-axis [45]. The total effective magnetic moment  $\mu_{eff}$  can be calculated by

$$\mu_{eff} = \frac{1}{\mu_B} \sqrt{\frac{3k_B M_R}{N_A \alpha}}, \quad (7)$$

where  $M_R$  is the molecular mass,  $N_A$  the Avogadro constant, and  $\alpha$  the slope of the linear fitting for  $\mu_0 \chi^{-1}$  vs.  $T$  [45].

**Figure 4** (c) plots the  $\mu_{eff}$  of all the samples. The total effective magnetic moment  $\mu_{eff}$  of (Nd,Pr)Al<sub>2</sub> increases roughly linearly with Pr content, whereas  $\mu_{eff}$  of (Pr,Ce)Al<sub>2</sub>

decreases with increasing Ce content. This observation can be explained by the fact that Pr<sup>3+</sup> has the largest magnetic moment of 3.58  $\mu_B$  and Ce<sup>3+</sup> has the smallest magnetic moment of 2.54  $\mu_B$  among the three light rare-earth ions.

**Figure 4** (d) plots the paramagnetic Curie temperature  $\theta_p$  and the *de Gennes* factor  $G$  of all the samples. The paramagnetic Curie temperature of (Nd,Pr)Al<sub>2</sub> decreases almost linearly with increasing Pr content, from 78.5 K for NdAl<sub>2</sub> to 32.6 K for PrAl<sub>2</sub>, and it is the same case with (Pr,Ce)Al<sub>2</sub>, from 32.6 K for PrAl<sub>2</sub> to 13.2 K for Pr<sub>0.5</sub>Ce<sub>0.5</sub>Al<sub>2</sub>. This agrees with the decreasing trend of the *de Gennes* factor from NdAl<sub>2</sub> to Pr<sub>0.5</sub>Ce<sub>0.5</sub>Al<sub>2</sub> since as Equation (6) indicates, smaller *de Gennes* factor, lower Curie temperature. The paramagnetic Curie temperature is in good agreement with the values of the Curie temperatures of NdAl<sub>2</sub> and PrAl<sub>2</sub> given by Ref. [70]. The reported Curie temperature for NdAl<sub>2</sub> varies from 65 to 82 K, and that for PrAl<sub>2</sub> varies from 31 to 38.5 K [70, 78, 83–85].

In conclusion, by tuning *de Gennes* factors via mixing different rare-earth elements, a fully light rare-earth based magnetocaloric material system with a paramagnetic Curie temperature covering the temperature range required for magnetocaloric hydrogen liquefaction (77 ~ 20 K) is developed. The large effective magnetic moments  $\mu_{eff}$  are retained from NdAl<sub>2</sub> to Pr<sub>0.75</sub>Ce<sub>0.25</sub>Al<sub>2</sub>.

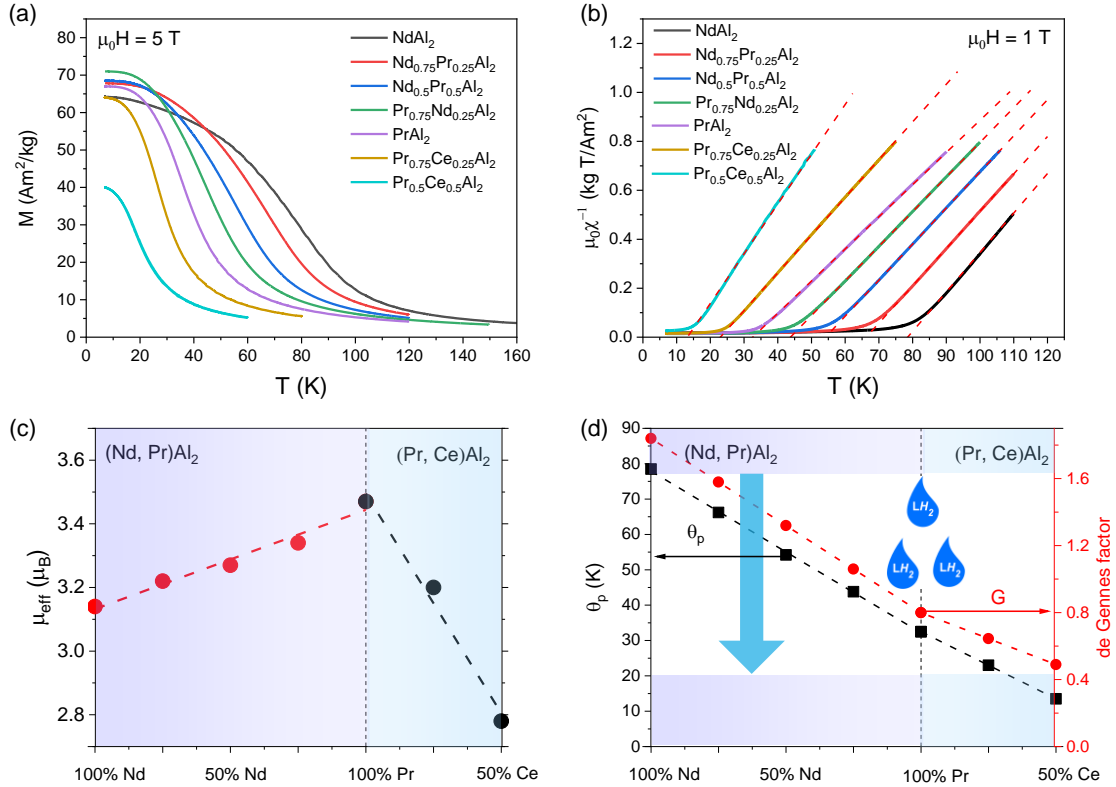


**Figure 4** (a) Magnetizations of the Laves phases (R<sub>1</sub>R<sub>2</sub>)Al<sub>2</sub> (R<sub>1</sub>: Nd, Pr, R<sub>2</sub>: Pr, Ce) as a function of temperature in magnetic fields of 5 T. (b) Curie-Weiss fits of the Laves phases (R<sub>1</sub>R<sub>2</sub>)Al<sub>2</sub> (R<sub>1</sub>: Nd, Pr, R<sub>2</sub>: Pr, Ce) in magnetic fields of 1 T. (c) Effective magnetic moments of the samples using the Curie-Weiss law. (d) Paramagnetic  $T_c$  of the samples determined by the Curie-Weiss law (black squares) and the average *de Gennes* factor (red circles).

### 4.3 Magnetocaloric effect

According to the theoretical calculations above, the maximum  $\Delta S_T$  of the light rare-earth based magnetocaloric materials are expected to be large in the vicinity of the condensation point of hydrogen (20 K). **Figure 5** (a) ~ (g) plot the  $\Delta S_T$  of all the samples in magnetic fields of 2 and 5 T.  $\Delta S_T(T, \Delta H)$  is determined by two methods: (1) heat capacity measurements under constant applied fields via the thermodynamic equation  $S(T, \Delta H) - S(T, 0) = \int_0^T \frac{C_p(T, \Delta H) - C_p(T, 0)}{T} dT$  ( $C_p$  is the isobaric heat capacity) [73, 86], (2) magnetization vs. fields measurements via the Maxwell relation  $\Delta S_T(T, \Delta H) = \int_{H_0}^{H_1} \frac{\partial M(H, T)}{\partial T} dH$  [37, 87, 88]. An example of how the  $\Delta S_T$  is calculated by these two methods for PrAl<sub>2</sub> is included in the supplementary. Both methods fit well, as the points of the  $\Delta S_T$  from magnetization measurements mostly lie on the lines of the  $\Delta S_T$  from heat capacity measurements. Besides, the temperatures where  $\Delta S_T$  peaks are close to the paramagnetic Curie temperatures, consistent with the feature that second-order magnetocaloric materials show a maximum  $\Delta S_T$  near their Curie temperatures [36, 65].

In agreement with the calculations in **Figure 2** (a) above, the maximum  $\Delta S_T$  increases from 7.21 J kg<sup>-1</sup> K<sup>-1</sup> for NdAl<sub>2</sub> to 18.53 J kg<sup>-1</sup> K<sup>-1</sup> for Pr<sub>0.75</sub>Ce<sub>0.25</sub>Al<sub>2</sub> in magnetic fields of 5 T, and from 3.67 J kg<sup>-1</sup> K<sup>-1</sup> for NdAl<sub>2</sub> to 10.48 J kg<sup>-1</sup> K<sup>-1</sup> for Pr<sub>0.75</sub>Ce<sub>0.25</sub>Al<sub>2</sub> in magnetic fields of 2 T. We observe an exception in this material series that Pr<sub>0.5</sub>Ce<sub>0.5</sub>Al<sub>2</sub> has a smaller maximum  $\Delta S_T$  than that of PrAl<sub>2</sub> and Pr<sub>0.75</sub>Ce<sub>0.25</sub>Al<sub>2</sub>. Similar observations were reported in RNi<sub>2</sub> (R: Gd, Tb, Dy, Ho, Er) [45, 71] and RAl<sub>2</sub> (R: Gd, Tb, Dy, Ho, Er, Tm) [72] series. One contribution to this decrease is the reduction of the effective magnetic moment  $\mu_{eff}$ . As revealed in **Figure 4** (c), Pr<sub>0.5</sub>Ce<sub>0.5</sub>Al<sub>2</sub> has the lowest  $\mu_{eff}$  in the series. Another contribution might be due to the fact that crystalline electric field has a considerable influence on the magnetocaloric effect in low temperatures [45]. In the case of Pr<sub>0.5</sub>Ce<sub>0.5</sub>Al<sub>2</sub>, the crystalline electric field may decrease the magnetic entropy change. However, this speculation needs to be validated.

**Figure 5** (h) and (i) compares the maximum  $\Delta S_T$  of the light rare-earth RAl<sub>2</sub> series in this work to some of the other light rare-earth magnetocaloric materials [89–94] and the heavy rare-earth RAl<sub>2</sub> (R: Tb, Dy, Ho, Er) and Tb<sub>x</sub>Ho<sub>1-x</sub>Ni<sub>2</sub> (x = 0.25, 0.5, 0.75, 1) series [45, 95, 96]. From the plots, we see

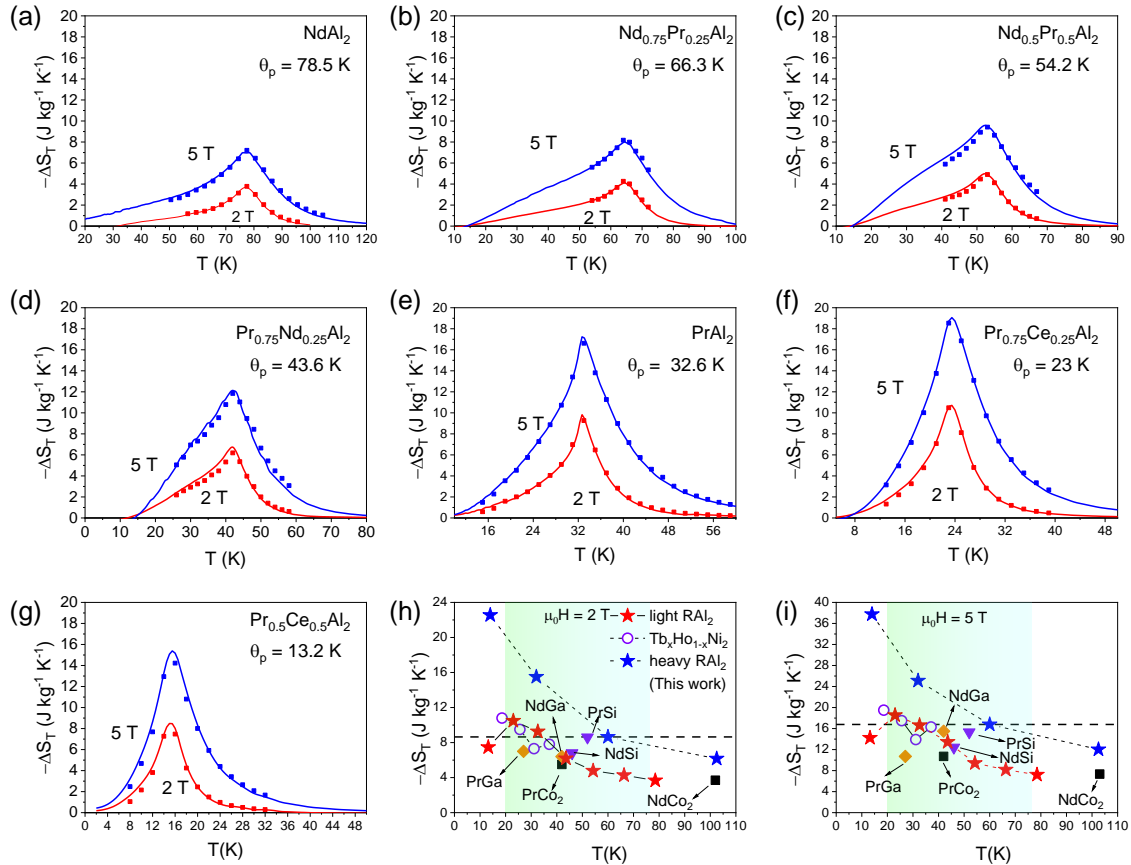


**Figure 5** (a) ~ (g)  $-\Delta S_T$  of (Nd, Pr)Al<sub>2</sub> and (Pr, Ce)Al<sub>2</sub> in magnetic fields of 2 T and 5 T. The solid lines are the  $-\Delta S_T$  calculated from heat capacity measurements, and the squares are the ones calculated from magnetization vs. magnetic field measurement. (h) ~ (i) Comparisons of the maximum  $-\Delta S_T$  of the light rare-earth series in this work, RCo<sub>2</sub> (Ref. [89, 90]), RSi (Ref. [91, 92]), and RGe (Ref. [93, 94]) where R = Pr, Nd, the heavy rare-earth based RAl<sub>2</sub> (Ref. [45, 95]) where R = Tb, Dy, Ho and Er, and Tb<sub>x</sub>Ho<sub>1-x</sub>Ni<sub>2</sub> (x = 0.75, 0.25, 0.5, 0) (Ref. [61]) in magnetic fields of 2 and 5 T. The green shadows mark the temperature range required for magnetocaloric hydrogen liquefaction (77 K ~ 20 K) and the black dashed lines highlight the values of DyAl<sub>2</sub>.

that the light rare-earth  $\text{RAl}_2$  series is highly competitive compared to the other light rare-earth magnetocaloric materials.  $\text{Pr}_{0.75}\text{Ce}_{0.25}\text{Al}_2$  exhibits the largest maximum  $\Delta S_T$  among all the light rare-earth magnetocaloric materials in **Figure 5** (h) and (i). The rest light rare-earth  $\text{RAl}_2$  samples show a maximum  $\Delta S_T$  that is larger than or comparable to the other light rare-earth compounds with a similar ordering temperature (except  $\text{PrSi}$  which shows a  $\Delta S_T$  larger than  $\text{PrAl}_2$  and  $\text{Pr}_{0.75}\text{Nd}_{0.25}\text{Al}_2$  samples).

Although the heavy rare-earth series  $\text{RAl}_2$  (R: Tb, Dy, Ho, Er) shows an obvious larger maximum  $\Delta S_T$  than their light rare-earth counterparts in the vicinity of their ordering temperatures, the light rare-earth  $\text{RAl}_2$  series exhibits large  $\Delta S_T$  near hydrogen condensation point (20 K), with  $\text{Pr}_{0.75}\text{Ce}_{0.25}\text{Al}_2$  having a larger  $\Delta S_T$  than  $\text{DyAl}_2$ , and  $\text{PrAl}_2$  having a significantly larger  $\Delta S_T$  than  $\text{TbAl}_2$ . Compared to other heavy rare-earth Laves phases such as  $\text{Tb}_x\text{Ho}_{1-x}\text{Ni}_2$  ( $x = 0.25, 0.5, 0.75, 1$ ) [45, 95, 96],  $\text{Pr}_{0.75}\text{Ce}_{0.25}\text{Al}_2$ ,  $\text{PrAl}_2$  and  $\text{Pr}_{0.75}\text{Nd}_{0.25}\text{Al}_2$  show a maximum  $\Delta S_T$  that is larger than or comparative to that of  $\text{Tb}_x\text{Ho}_{1-x}\text{Ni}_2$ .

Adiabatic temperature change  $\Delta T_{ad}$  is as important as  $\Delta S_T$  for magnetocaloric effect. **Figure 6** (a)~(g) plot the  $\Delta T_{ad}$  of the light rare-earth  $\text{RAl}_2$  samples determined by equation

(5) via constructing the  $S(H, T)$  curves from the heat capacity measurements in magnetic fields of 0, 2, and 5 T. In agreement with the theoretical calculations above, the maximum  $\Delta T_{ad}$  of the light rare-earth  $\text{RAl}_2$  series is large in the vicinity of the condensation point of hydrogen (20 K), with all the three (Pr,Ce) $\text{Al}_2$  samples showing a maximum  $\Delta T_{ad}$  over 2 K in magnetic fields of 2 T. In 5 T, all the three (Pr,Ce) $\text{Al}_2$  samples have a maximum adiabatic temperature change over 4 K, and  $\text{Pr}_{0.75}\text{Ce}_{0.25}\text{Al}_2$  even shows a value close to 5 K. **Figure 6** (h)~(i) compares the maximum  $\Delta T_{ad}$  of the light- and heavy rare-earth  $\text{RAl}_2$ , and the Laves phases  $\text{Tb}_x\text{Ho}_{1-x}\text{Ni}_2$ . The light rare-earth  $\text{RAl}_2$  shows a maximum  $\Delta T_{ad}$  which is about  $1/3 \sim 1/2$  of the maximum values of the heavy rare-earth  $\text{RAl}_2$  in the vicinity of their ordering temperatures. Compared to  $\text{Tb}_x\text{Ho}_{1-x}\text{Ni}_2$  [45, 95, 96] in magnetic fields of 2 T,  $\text{PrAl}_2$  and  $\text{Pr}_{0.75}\text{Nd}_{0.25}\text{Al}_2$  show a maximum  $\Delta T_{ad}$  that is about half of the values of  $\text{HoNi}_2$  and  $\text{Tb}_{0.25}\text{Ho}_{0.75}\text{Ni}_2$ , but comparative to that of  $\text{Tb}_{0.5}\text{Ho}_{0.5}\text{Ni}_2$  and  $\text{Tb}_{0.75}\text{Ho}_{0.25}\text{Ni}_2$ .

In summary, the light rare-earth  $\text{RAl}_2$  alloy series shows a large  $\Delta S_T$  being comparable to the other light rare-earth based materials in **Figure 5** (h) and (i). Both of their  $\Delta S_T$  and  $\Delta T_{ad}$  show a large maximum value near 20 K. Despite showing a smaller  $\Delta S_T$  and  $\Delta T_{ad}$  than their heavy rare-earth

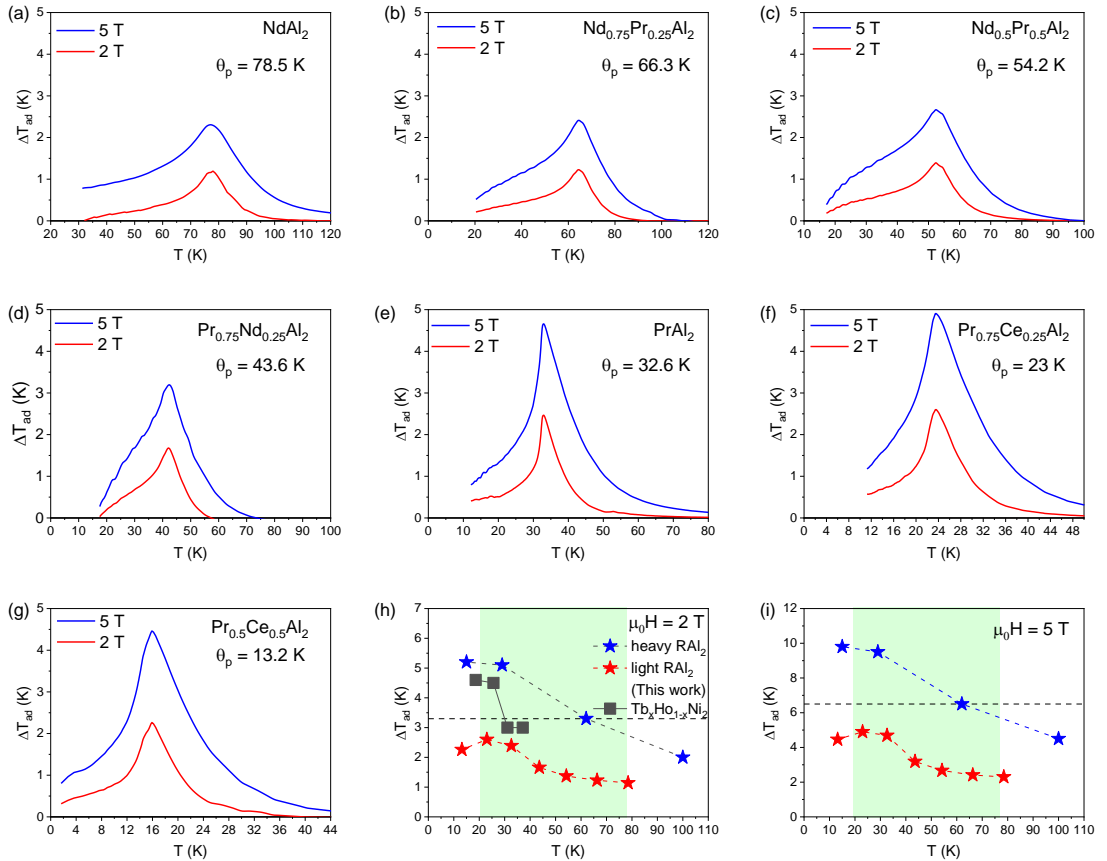


**Figure 6** (a)~(g)  $\Delta T_{ad}$  of  $(\text{R}_1, \text{R}_2)\text{Al}_2$  ( $\text{R}_1$ : Nd, Pr,  $\text{R}_2$ : Pr, Ce) determined from heat capacity measurements in magnetic fields of 2 and 5 T. (h)~(i) comparisons of the  $\Delta T_{ad}$  of the light- and heavy rare-earth  $\text{RAl}_2$  series, and the  $\text{Tb}_x\text{Ho}_{1-x}\text{Ni}_2$  ( $x = 0.75, 0.25, 0.5, 0$ ) (data of heavy rare-earth  $\text{RAl}_2$  (R = Tb, Dy, Ho, and Er) and  $\text{Tb}_x\text{Ho}_{1-x}\text{Ni}_2$  are taken from Ref. 45 and 61, respectively). The green shadows mark the temperature range required for magnetocaloric hydrogen liquefaction (77 K ~ 20 K) and the black dashed lines highlight the values of  $\text{DyAl}_2$ .

counterparts in the vicinity of their ordering temperatures, we see a high potential of the light rare-earth  $\text{RAI}_2$  series for magnetocaloric hydrogen liquefaction, especially near 20 K, the condensation point of hydrogen.

## 5. Conclusions

The relatively high abundance of light rare-earth elements in the earth's crust makes their alloys appealing for magnetocaloric hydrogen liquefaction on an industrial scale. In this work, we aimed at designing a fully light rare-earth based magnetocaloric material system covering the full temperature range from 77 to 20 K required by hydrogen liquefaction.

In order to formulate a strategy for alloy design, the mean-field approach shown in our previous work is further developed to be applied to the light rare-earth alloys. From the theoretical analysis, we see that if  $T_C$  of a light rare-earth based magnetocaloric material is tuned towards lower cryogenic temperature, the magnetocaloric effect is supposed to become stronger. Especially in the vicinity of the condensation point of hydrogen, the mean-field approach predicts significantly large  $\Delta S_T$  and  $\Delta T_{ad}$ . Based on these observations and taking the chemical and physical similarities of the light rare-earth elements, a design strategy for developing light rare-earth material series for hydrogen liquefaction is used: tune the  $T_C$  by mixing the light rare-earth elements with different de Gennes factors.

Consequently, a light rare-earth  $\text{RAI}_2$  Laves phase series with the ordering temperatures covering the temperature range from 77 to 20 K is successfully developed. This material series exhibits large  $\Delta S_T$ . Especially near 20 K (condensation point of hydrogen), the  $(\text{Pr}_x, \text{Ce}_{1-x})\text{Al}_2$  ( $x = 0, 0.75, 0.5$ ) samples show a  $\Delta S_T$  that is larger than or comparable to that of  $\text{DyAl}_2$ , a heavy rare-earth based magnetocaloric material which is often proposed to be used in an active regenerator for hydrogen liquefaction [32]. Large  $\Delta T_{ad}$  in the vicinity of 20 K are achieved in the  $(\text{Pr}_{1-x}\text{Ce}_x)\text{Al}_2$  ( $x = 0, 0.75, 0.5$ ) samples, which show a value that is more than two third of that of  $\text{DyAl}_2$ .

This design strategy for designing the light rare-earth  $\text{RAI}_2$  Laves phase series for magnetocaloric hydrogen liquefaction may be applied to other light rare-earth alloys to tailor their magnetocaloric effects for the liquefaction of industrial gases, inclusive but not limited to hydrogen gas. In addition, our work is also helpful for designing magnetocaloric composites, since tuning the Curie temperature in layered structures with a constant  $\Delta S_T$  over a wide temperature range is important for applications [60, 62].

## 6. Acknowledgement

We appreciate the financial supports from Helmholtz Association via the Helmholtz-RSF Joint Research Group (Project No. HRSF-0045), from the HLD at HZDR (member

of the European Magnetic Field Laboratory (EMFL)). We further gratefully acknowledge supports from the DFG through the Würzburg-Dresden Cluster of Excellence on Complexity and Topology in Quantum Matter-*ct.qmat* (EXC 2147, Project ID 39085490), the CRC/TRR 270 (Project-ID 405553726) and the Project-ID 456263705, from the ERC under the European Union's Horizon 2020 research and innovation program (Grant No. 743116, Cool Innov), and the Clean Hydrogen Partnership and its members within the framework of the project HyLICAL (Grant No. 101101461).

## 7. Data availability statements

The data that support the findings of this study are available upon reasonable request from the authors.

## 8. References

- [1] Smith A 2013 Who discovered the magnetocaloric effect? *Eur. Phys. J. H* **38** 507–17
- [2] Giauque W F 1927 A thermodynamic treatment of magnetic effects. A proposed method of producing temperatures below  $1^\circ$  absolute *J. Am. Chem. Soc.* **49** 1864–70
- [3] Debye P 1926 Einige Bemerkungen zur Magnetisierung bei tiefer Temperatur *Ann. Phys.* **386** 1154–60
- [4] Shampo M A, Kyle R A and Steensma D P 2006 Stamp vignette on medical science. William F. Giauque--Nobel Prize for low-temperature research *Mayo Clin. Proc.* **81** 587
- [5] Gutfleisch O, Willard M A, Brück E, Chen C H, Sankar S G and Liu J P 2011 Magnetic materials and devices for the 21st century: stronger, lighter, and more energy efficient *Adv. Mater.* **23** 821–42
- [6] Glenk G and Reichelstein S 2019 Economics of converting renewable power to hydrogen *Nat. Energy* **4** 216–22
- [7] Züttel A, Remhof A, Borgschulte A and Friedrichs O 2010 Hydrogen: the future energy carrier *Philos. Trans. R. Soc. A-Math. Phys. Eng. Sci.* **368** 3329–42
- [8] Sazali N 2020 Emerging technologies by hydrogen: A review *Int. J. Hydrog. Energy* **45** 18753–71
- [9] Durbin D J and Malardier-Jugroot C 2013 Review of hydrogen storage techniques for on board vehicle applications *Int. J. Hydrog. Energy* **38** 14595–617
- [10] Aziz M 2021 Liquid hydrogen: a review on liquefaction, storage, transportation, and safety *Energies* **14** 5917
- [11] Heuser P-M, Ryberg D S, Grube T, Robinius M and Stolten D 2019 Techno-economic analysis of a potential energy trading link between Patagonia and Japan based on  $\text{CO}_2$  free hydrogen *Int. J. Hydrog. Energy* **44** 12733–47
- [12] Kamiya S, Nishimura M and Harada E 2015 Study on introduction of  $\text{CO}_2$  free energy to Japan with liquid hydrogen *Physics Procedia* **67** 11–9
- [13] Yang S *et al* 2023 Giant low-field magnetocaloric effect in ferromagnetically ordered  $\text{Er}_{1-x}\text{Tm}_x\text{Al}_2$  ( $0 \leq x \leq 1$ ) compounds *J. Mater. Sci. Technol.* **146** 168–76

- [14] Tang X *et al* 2022 Magnetic refrigeration material operating at a full temperature range required for hydrogen liquefaction *Nat. Commun.* **13** 1817
- [15] Terada N and Mamiya H 2021 High-efficiency magnetic refrigeration using holmium *Nat. Commun.* **12** 1212
- [16] Liu W, Scheibel F, Gottschall T, Bykov E, Dirba I, Skokov K and Gutfleisch O 2021 Large magnetic entropy change in Nd<sub>2</sub>In near the boiling temperature of natural gas *Appl. Phys. Lett.* **119** 22408
- [17] Yang S X *et al* 2022 Large magnetocaloric effect of Tm<sub>1-x</sub>Y<sub>x</sub> Ga (0 ≤ x ≤ 0.8) compounds with second-order magnetic transition around liquid helium temperature *J. Appl. Phys.* **131** 185110
- [18] Biswas A, Del Rose T, Mudryk Y, Ribeiro P O, Alho B P, Sousa V de, Nóbrega E P, Ranke P J von and Pecharsky V K 2022 Hidden first-order phase transitions and large magnetocaloric effects in GdNi<sub>1-x</sub>Co<sub>x</sub> *J. Alloy. Compd.* **897** 163186
- [19] Lai J, Bolyachkin A, Terada N, Dieb S, Tang X, Ohkubo T, Sepehri-Amin H and Hono K 2022 Machine learning assisted development of Fe<sub>2</sub>P-type magnetocaloric compounds for cryogenic applications *Acta Mater.* **232** 117942
- [20] Lai J, Sepehri-Amin H, Tang X, Li J, Matsushita Y, Ohkubo T, Saito A T and Hono K 2021 Reduction of hysteresis in (La<sub>1-x</sub>Ce<sub>x</sub>)<sub>y</sub> (Mn<sub>z</sub> Fe<sub>11.4-z</sub>)Si<sub>1.6</sub> magnetocaloric compounds for cryogenic magnetic refrigeration *Acta Mater.* **220** 117286
- [21] Ribeiro P O, Alho B P, Oliveira R S de, Nóbrega E P, Sousa V de, Ranke P J von, Biswas A, Khan M, Mudryk Y and Pecharsky V K 2022 Magnetothermal properties of Ho<sub>1-x</sub>Dy<sub>x</sub>Al<sub>2</sub> (x = 0, 0.05, 0.10, 0.15, 0.25 and 0.50) compounds *J. Magn. Magn. Mater.* **544** 168705
- [22] Xie H, Su W, Lu H, Mo Z, Wang D, Sun H, tian L, Gao X, Li Z and Shen J 2022 Enhanced low-field magnetocaloric effect in Nb and Al co-substituted EuTiO<sub>3</sub> compounds *J. Mater. Sci. Technol.* **118** 128–35
- [23] Ma Z, Dong X, Zhang Z and Li L 2021 Achievement of promising cryogenic magnetocaloric performances in La<sub>1-x</sub>Pr<sub>x</sub> Fe<sub>12</sub>B<sub>6</sub> compounds *J. Mater. Sci. Technol.* **92** 138–42
- [24] Zhang Z, Xu P, Jia Y and Li L 2023 Structural, magnetic and magnetocaloric properties in distorted RE<sub>2</sub>NiTiO<sub>6</sub> double perovskite compounds *J. Phys. Energy* **5** 14017
- [25] Biswas A, Chouhan R K, Thayer A, Mudryk Y, Hlova I Z, Dolotko O and Pecharsky V K 2022 Unusual first-order magnetic phase transition and large magnetocaloric effect in Nd<sub>2</sub>In *Phys. Rev. Materials* **6**
- [26] Lyubina J 2017 Magnetocaloric materials for energy efficient cooling *J. Phys. D: Appl. Phys.* **50** 53002
- [27] Masche M, Liang J, Engelbrecht K and Bahl C 2022 Performance assessment of a rotary active magnetic regenerator prototype using gadolinium *Appl. Therm. Eng.* **204** 117947
- [28] Feng T, Chen R and Ihnfeldt R V 2020 Modeling of hydrogen liquefaction using magnetocaloric cycles with permanent magnets *Int. J. Hydrog. Energy* **119** 238–46
- [29] Moya X, Kar-Narayan S and Mathur N D 2014 Caloric materials near ferroic phase transitions *Nat. Mater.* **13** 439–50
- [30] Moya X, Defay E, Heine V and Mathur N D 2015 Too cool to work *Nat. Phys.* **11** 202–5
- [31] Kamiya K 2006 Design and build of magnetic refrigerator for hydrogen liquefaction *AIP Conference Proceedings ADVANCES IN CRYOGENIC ENGINEERING: Transactions of the Cryogenic Engineering Conference - CEC (Keystone, Colorado (USA), 29 August-2 Septembe)* (AIP) pp 591–7
- [32] Kamiya K *et al* 2022 Active magnetic regenerative refrigeration using superconducting solenoid for hydrogen liquefaction *Appl. Phys. Express* **15** 53001
- [33] Gottschall T, Skokov K P, Fries M, Taubel A, Radulov I, Scheibel F, Benke D, Riegg S and Gutfleisch O 2019 Making a cool choice: the materials library of magnetic refrigeration *Adv. Energy Mater.* **9** 1901322
- [34] Balli M, Jandl S, Fournier P and Kedous-Lebouc A 2017 Advanced materials for magnetic cooling: Fundamentals and practical aspects *Appl. Phys. Rev.* **4** 21305
- [35] Kitanovski A 2020 Energy applications of magnetocaloric materials *Adv. Energy Mater.* **10** 1903741
- [36] Smith A, Bahl C R, Bjørk R, Engelbrecht K, Nielsen K K and Pryds N 2012 materials challenges for high performance magnetocaloric refrigeration devices *Adv. Energy Mater.* **2** 1288–318
- [37] Franco V, Blázquez J S, Ipus J J, Law J Y, Moreno-Ramírez L M and Conde A 2018 Magnetocaloric effect: From materials research to refrigeration devices *Prog. Mater. Sci.* **93** 112–232
- [38] Gutfleisch O *et al* 2016 Mastering hysteresis in magnetocaloric materials *Philos. Trans. R. Soc. A-Math. Phys. Eng. Sci.* **374**
- [39] Zheng X-Q and Shen B-G 2017 The magnetic properties and magnetocaloric effects in binary R – T (R = Pr, Gd, Tb, Dy, Ho, Er, Tm; T = Ga, Ni, Co, Cu) intermetallic compounds *Chin. Phys. B (Chinese Physics B)* **26** 27501
- [40] Zhang H and Shen B-G 2015 Magnetocaloric effects in RTX intermetallic compounds (R = Gd–Tm, T = Fe–Cu and Pd, X = Al and Si) *Chin. Phys. B* **24** 127504
- [41] Castro P B de, Terashima K, Yamamoto T D, Iwasaki S, Matsumoto R, Adachi S, Saito Y, Takeya H and Takano Y 2021 Effect of Dy substitution in the giant magnetocaloric properties of HoB<sub>2</sub> *Sci. Technol. Adv. Mater.* **21** 849–55
- [42] Li J, Liu Y, Lu X, Zhang Y, Guo J, Zhang M and Liu J 2021 Enhanced refrigeration capacity in Ho<sub>1-x</sub>Dy<sub>x</sub>B<sub>2</sub> compounds around liquid hydrogen temperature *J. Alloy. Compd.* **864** 158757
- [43] Oliveira N A de, Ranke P J von, Tovar Costa M V and Troper A 2002 Magnetocaloric effect in the intermetallic compounds RCo<sub>2</sub> (R=Dy, Ho, Er) *Phys. Rev. B* **66**
- [44] Lu G Y, Du Y S, Wu X F, Ma L, Li L, Cheng G, Wang J, Zhao J T and Rao G H 2022 Effect of Cu substitution on the type of magnetic phase transition and magnetocaloric effect in the ErCo<sub>2-x</sub>Cu<sub>x</sub> compounds *J. Alloy. Compd.* **906** 164343
- [45] Liu W *et al* 2022 A study on rare-earth Laves phases for

- magnetocaloric liquefaction of hydrogen *Appl. Mater. Today* **29** 101624
- [46] Oliveira N A de and Ranke P J von 2008 Magnetocaloric effect in the Laves phase pseudobinaries  $Dy_{1-x}R_xAl_2$  ( $R=Er$  and  $Ho$ ) *J. Magn. Magn. Mater.* **320** 386–92
- [47] Coey J M D 2009 *Magnetism and magnetic materials* (New York, USA: Cambridge university press)
- [48] Fuel Cells and Hydrogen 2 Joint Undertaking. 2019 *Hydrogen roadmap Europe: a sustainable pathway for the European energy transition*, Publication Office, <https://data.europa.eu/doi/10.2843/341510> (Luxembourg)
- [49] Bykov E et al 2021 Magnetocaloric effect in the Laves-phase  $Ho_{1-x}Dy_xAl_2$  family in high magnetic fields *Phys. Rev. Mater.* **5**
- [50] <https://mmta.co.uk/metals/ho/>
- [51] European Commission, Directorate-General for Internal Market, Industry, Entrepreneurship and SMEs, Bobba S, Carrara S, Huisman J, Mathieux F and Pavel C 2020 *Critical raw materials for strategic technologies and sectors in the EU: a foresight study*, Publications Office, <https://data.europa.eu/doi/10.2873/58081>
- [52] Liao X et al 2022 Textured (Ce,La,Y)–Fe–B permanent magnets by hot deformation *J. Mater. Res. Technol.* **17** 1459–68
- [53] Yaroshevsky A A 2006 Abundances of chemical elements in the Earth's crust *Geochem. Int.* **44** 48–55
- [54] U.S. Geological Survey 2022 *Mineral commodity summaries* 2022 <http://pubs.er.usgs.gov/publication/mcs2022>
- [55] Gielen D and Lyons M 2022 *Critical materials for the energy transition: Rare earth elements* <https://www.irena.org/Technical-Papers/Critical-Materials-For-The-Energy-Transition-Rare-Earth-elements>
- [56] Gauß R, Burkhardt C, Carencotte F, Gasparon M, Gutfleisch O, Higgins I, Karajić M, Klossek A, Mäkinen M and Schäfer B 2021 *Rare earth magnets and motors: A European call for action* (Berlin 2021: Rare Earth Magnets and Motors Cluster of the European Raw Materials Alliance)
- [57] Gauß R, Homm G and Gutfleisch O 2017 The resource basis of magnetic refrigeration *J. Ind. Ecol.* **21** 1291–300
- [58] Gauß R and Gutfleisch O 2016 Magnetische Materialien — Schlüsselkomponenten für neue Energietechnologien *Rohstoffwirtschaft und gesellschaftliche Entwicklung: Die nächsten 50 Jahre* ed P Kausch et al (Berlin, Heidelberg: Springer Berlin Heidelberg) pp 99–118
- [59] Ćwik J, Koshkid'ko Y, Nenkov K, Mikhailova A, Małecka M, Romanova T, Kolchugina N and Oliveira N A de 2021 Experimental and theoretical analysis of magnetocaloric behavior of  $Dy_{1-x}Er_xNi_2$  intermetallics ( $x=0.25,0.5,0.75$ ) and their composites for low-temperature refrigerators performing an Ericsson cycle *Phys. Rev. B* **103**
- [60] Ćwik J, Koshkid'ko Y, Nenkov K, Tereshina-Chitrova E, Weise B and Kowalska K 2022 Low-Temperature Magnetothermodynamics Performance of  $Tb_{1-x}Er_xNi_2$  Laves-Phases Compounds for Designing Composite Refrigerants *Crystals* **12** 931
- [61] Ćwik J, Koshkid'ko Y, Małecka M, Weise B, Krautz M, Mikhailova A and Kolchugina N 2021 Magnetocaloric prospects of mutual substitutions of rare-earth elements in pseudobinary  $Tb_{1-x}Ho_xNi_2$  compositions ( $x = 0.25–0.75$ ) *J. Alloy. Compd.* **886** 161295
- [62] Ćwik J, Koshkid'ko Y, Nenkov K, Tereshina-Chitrova E, Małecka M, Weise B and Kowalska K 2022 Magnetocaloric performance of the three-component  $Ho_{1-x}Er_xNi_2$  ( $x = 0.25, 0.5, 0.75$ ) Laves phases as composite refrigerants *Scientific reports* **12** 12332
- [63] Zhu Y, Asamoto K, Nishimura Y, Kouen T, Abe S, Matsumoto K and Numazawa T 2011 Magnetocaloric effect of  $(Er_xR_{1-x})Co_2$  ( $R=Ho, Dy$ ) for magnetic refrigeration between 20 and 80K *Cryogenics* **51** 494–8
- [64] Mudryk Y, Alho B P, Ribeiro P O and Pecharsky V K 2020 Low-Temperature Crystal Structure and Mean-Field Modeling of  $Er_xDy_{1-x}Al_2$  Intermetallics *Metals* **10** 1662
- [65] Franco V, Conde A, Kuz'min M D and Romero-Enrique J M 2009 The magnetocaloric effect in materials with a second order phase transition: Are TC and Tpeak necessarily coincident? *J. Appl. Phys.* **105** 07A917
- [66] Gottschall T et al 2019 Magnetocaloric effect of gadolinium in high magnetic fields *Phys. Rev. B* **99**
- [67] Belo J H, Amaral J S, Pereira A M, Amaral V S and Araújo J P 2012 On the Curie temperature dependency of the magnetocaloric effect *Appl. Phys. Lett.* **100** 242407
- [68] Romero-Muñiz C, Tamura R, Tanaka S and Franco V 2016 Applicability of scaling behavior and power laws in the analysis of the magnetocaloric effect in second-order phase transition materials *Phys. Rev. B* **94**
- [69] Oesterreicher H and Parker F T 1984 Magnetic cooling near Curie temperatures above 300 K *J. Appl. Phys.* **55** 4334–8
- [70] Carvalho A M G, Campoy J C P, Coelho A A, Plaza E J R, Gama S and Ranke P J von 2005 Experimental and theoretical analyses of  $PrAl_2$  and  $NdAl_2$  composite for use as an active magnetic regenerator *J. Appl. Phys.* **97** 83905
- [71] Ranke P J von, Grangeia D F, Caldas A and Oliveira N A de 2003 Investigations on magnetic refrigeration: Application to  $RNi_2$  ( $R=Nd, Gd, Tb, Dy, Ho, and Er$ ) *J. Appl. Phys.* **93** 4055–9
- [72] Ranke P von, Oliveira N de, Tovar Costa M, Nobrega E, Caldas A and Oliveira I de 2001 The influence of crystalline electric field on the magnetocaloric effect in the series  $RA_2$  ( $R=Pr, Nd, Tb, Dy, Ho, Er, and Tm$ ) *J. Magn. Magn. Mater.* **226** 970–2
- [73] Tishin A M and Spichkin Y I 2003 *The magnetocaloric effect and its applications (Series in condensed matter physics)* (Bristol, Philadelphia: Institute of Physics Pub)
- [74] Kittel C and McEuen P 2018 *Introduction to solid state physics* (Hoboken, NJ: Wiley)
- [75] Hungsberg R E and Gschneidner K A 1972 Low temperature heat capacity of some rare earth aluminum Laves phase compounds:  $YAl_2, LaAl_2$  and  $LuAl_2$  *J. Phys.*

- Chem. Solids* **33** 401–7
- [76] Hirayama Y, Nakagawa T and Yamamoto T A 2011 Curie temperatures and modified de Gennes factors of rare earth nitrides *Solid State Commun.* **151** 1602–4
- [77] Pszczoła J 2021 Curie temperatures of substituted rare earth-Aluminium  $L_{1-x}R_xAl_2$  compounds *Acta Phys. Pol. A* **140** 72–7
- [78] Swift W M and Wallace W E 1968 Magnetic characteristics of laves phase compounds containing two lanthanides with aluminum *J. Phys. Chem. Solids* **29** 2053–61
- [79] Rodríguez-Carvajal J 1993 Recent advances in magnetic structure determination by neutron powder diffraction *Physica B* **192** 55–69
- [80] Mudryk Y, Pecharsky V K and Gschneidner K A 2014 Chapter 262 - R5T4 Compounds: An Extraordinary Versatile Model System for the Solid State Science *Handbook on the Physics and Chemistry of Rare Earths : Including Actinides* ed J-C G Bünzli and V K Pecharsky (Elsevier) pp 283–449
- [81] Mugiraneza S and Hallas A M 2022 Tutorial: a beginner's guide to interpreting magnetic susceptibility data with the Curie-Weiss law *Commun. Phys.* **5**
- [82] Pöttgen R 2014 Chapter 315 - The Gd<sub>4</sub>RhIn type: Crystal chemistry and properties *Handbook on the Physics and Chemistry of Rare Earths : Including Actinides* ed J-C G Bünzli and V K Pecharsky (Elsevier) pp 1–38
- [83] Nereson N, Olsen C and Arnold G 1966 Magnetic Properties of DyAl<sub>2</sub> and NdAl<sub>2</sub> *J. Appl. Phys.* **37** 4575–80
- [84] Nereson N, Olsen C and Arnold G 1968 Magnetic Properties of PrAl<sub>2</sub> and ErAl<sub>2</sub> *J. Appl. Phys.* **39** 4605–9
- [85] Mader K, Segal E and Wallace W 1969 Magnetic and crystallographic characteristics of (Pr,La)Al<sub>3</sub>, (Pr,Y)Al<sub>3</sub>, (Pr,La)Al<sub>2</sub> and (Pr,Y)Al<sub>2</sub> *J. Phys. Chem. Solids* **30** 1–12
- [86] Bratko M, Morrison K, Campos A de, Gama S, Cohen L F and Sandeman K G 2012 History dependence of directly observed magnetocaloric effects in (Mn, Fe)As *Appl. Phys. Lett.* **100** 252409
- [87] Sandeman K G 2012 Magnetocaloric materials: The search for new systems *Scr. Mater.* **67** 566–71
- [88] Amaral J S and Amaral V S 2010 On estimating the magnetocaloric effect from magnetization measurements *J. Magn. Magn. Mater.* **322** 1552–7
- [89] Murtaza A *et al* 2020 Magnetocaloric effect in the vicinity of the magnetic phase transition in NdCo<sub>2-x</sub>Fe<sub>x</sub> compounds *Phys. Rev. B* **101**
- [90] Dong P L, Ma L, Xiong J C, Chen T Y, Lu S F and Li L 2019 Effect of Dy addition on magnetocaloric effect in PrCo<sub>2</sub> compound *Mater. Res. Express* **6** 126102
- [91] Zhang Q M, Gao R L, Cui L, Wang L C, Fu C L, Xu Z Y, Mo Z J, Cai W, Chen G and Deng X L 2015 Magnetic properties and magnetocaloric effect of the compound NdSi *Physica B* **456** 258–60
- [92] Wang L-C and Shen B-G 2014 Magnetic properties and magnetocaloric effects of PrSi *Rare Met.* **33** 239–43
- [93] Zheng X Q, Xu J W, Shao S H, Zhang H, Zhang J Y, Wang S G, Xu Z Y, Wang L C, Chen J and Shen B G 2018 Large magnetocaloric effect of NdGa compound due to successive magnetic transitions *AIP Adv.* **8** 56425
- [94] Zheng X Q, Chen J, Xu Z Y, Mo Z J, Hu F X, Sun J R and Shen B G 2014 Nearly constant magnetic entropy change and adiabatic temperature change in PrGa compound *J. Appl. Phys.* **115** 17A938
- [95] Khan M, Gschneidner K A and Pecharsky V K 2011 Spin reorientation transitions in Ho<sub>1-x</sub>Dy<sub>x</sub>Al<sub>2</sub> alloys *J. Appl. Phys.* **110** 103912
- [96] Gil L A, Campoy J, Plaza E and Souza M V de 2016 Conventional and anisotropic magnetic entropy change in HoAl<sub>2</sub> ferromagnetic compound *J. Magn. Magn. Mater.* **409** 45–9

## Supplementary

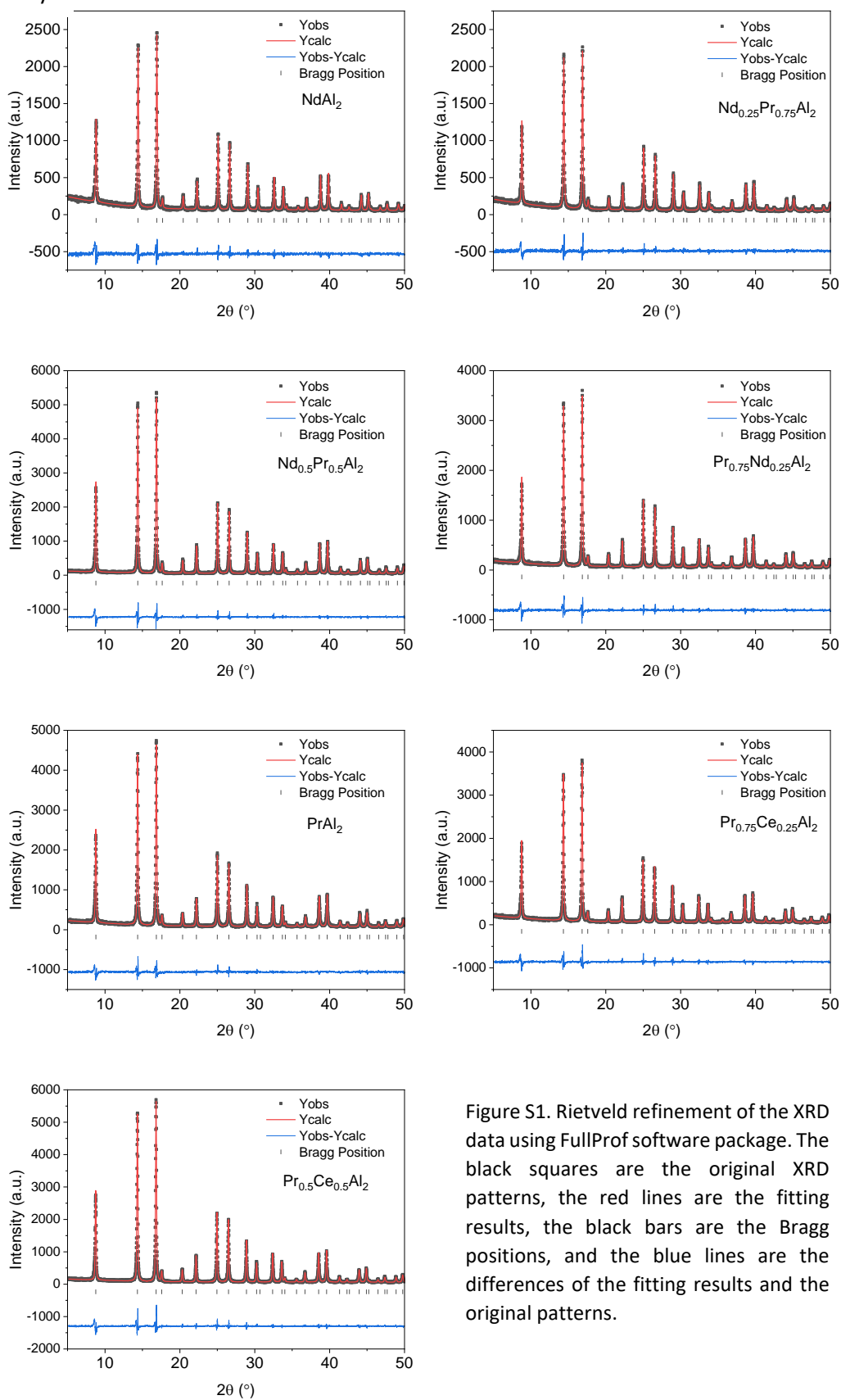


Figure S1. Rietveld refinement of the XRD data using FullProf software package. The black squares are the original XRD patterns, the red lines are the fitting results, the black bars are the Bragg positions, and the blue lines are the differences of the fitting results and the original patterns.

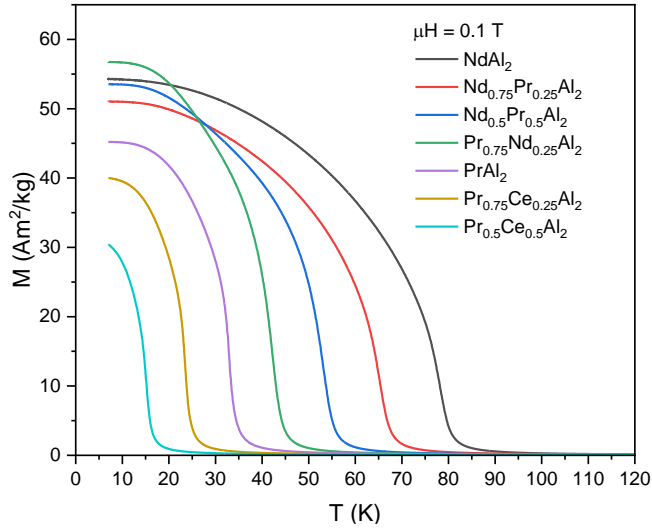


Figure S2. Magnetization as a function of temperatures for all the light rare-earth  $RAl_2$  samples in magnetic fields of 0.1 T.

As shown in Figure S3, the total entropy  $S(T)$  curves of  $PrAl_2$  in magnetic fields of 0, 2, and 5 T were constructed by the heat capacity measurements via the equation  $S(T) = \int_0^T \frac{C_p}{T} dT$ . The  $\Delta S_T$  and  $\Delta T_{ad}$  from the heat capacity measurements were calculated by the equation (5) shown in the main article.

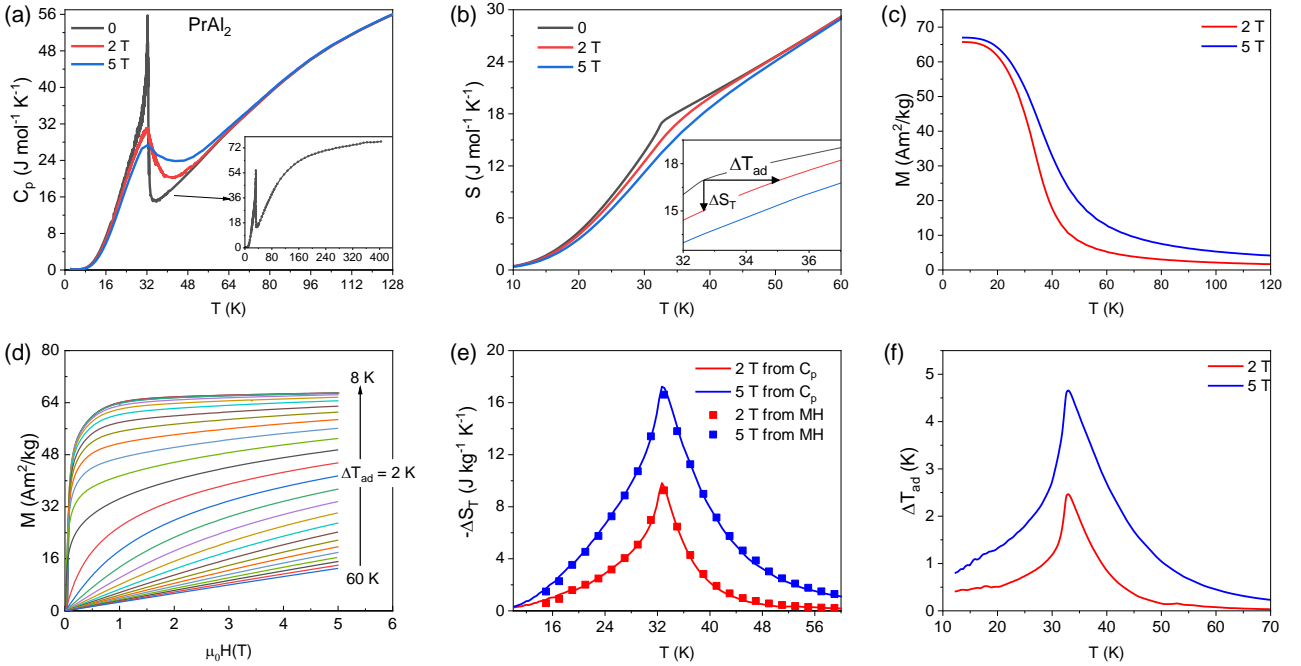


Figure S3. (a) heat capacity of  $PrAl_2$  measured in 0, 2, and 5 T. The inset shows the heat capacity in zero fields up to 404 K. (b)  $S(T)$  curves of  $PrAl_2$  in magnetic fields of 0, 2, and 5 T. The inset shows the curves in temperature range of 32 ~ 37 K. (c) Magnetization of  $PrAl_2$  as a function of temperature in magnetic fields of 2 and 5 T. (d) Magnetization of  $PrAl_2$  as a function of magnetic fields at a constant temperature from 8 K to 60 K with a step of 2 K. (e) Isothermal magnetic entropy change of  $PrAl_2$ . The solid lines are calculated from heat capacity measurements while the squares are calculated from magnetization vs. magnetic field (MH) at a constant temperature. (f) adiabatic temperature change of  $PrAl_2$  calculated from heat capacity measurements.